

**Supporting information -  $^{89}\text{Zr}$ -PET imaging of double DNA strand breaks for the early monitoring of response following  $\alpha$ - and  $\beta$ -particle radioimmunotherapy in a mouse model of pancreatic ductal adenocarcinoma**

Sophie Poty<sup>1\*</sup>, Komal Mandeylwala<sup>1</sup>, Edward O'Neill<sup>2</sup>, James Knight<sup>2</sup>, Bart Cornelissen<sup>2</sup>, Jason S. Lewis<sup>1\*</sup>.

<sup>1</sup> Department of Radiology, Memorial Sloan Kettering Cancer Center, NY, USA

<sup>2</sup> CRUK/MRC Oxford Institute of Radiation Oncology, Department of Oncology, University of Oxford, Oxford, UK

<sup>3</sup> Radiochemistry and Molecular Imaging Probes Core, Memorial Sloan Kettering Cancer Center, New York, NY, USA

<sup>4</sup> Department of Pharmacology, Weill Cornell Medical College, New York, NY, USA

<sup>5</sup> Molecular Pharmacology Program, Memorial Sloan Kettering Cancer Center, New York, NY, USA

<sup>6</sup> Department of Radiology, Weill Cornell Medical College, New York, NY, USA

## Methods

### *Relative biological effectiveness calculation*

The relative biological effectiveness (RBE) was calculated based on 48 hours in vitro cytotoxicity experiments as followed:

$$RBE = \frac{\text{Ratio of cytotoxicity}}{\text{Ratio of total particle energy per decay at 48 hours}}$$

The ratio of total particle energy per day is calculated taking into account the different physical properties of lutetium-177 and actinium-225 as followed:

- Lutetium-177 ( $t_{1/2} = 6.7$  days, total energy per decay = 0.147 MeV)

- Actinium-225 ( $t_{1/2} = 9.9$  days, total energy per decay [including decay daughters] = 28.16 MeV)

$$\begin{aligned} \text{Ratio (48 hours)} &= \frac{{}^{225}\text{Ac total energy per decay (48 hours)}}{{}^{177}\text{Lu total energy per decay (48 hours)}} \\ &= \frac{5.688}{0.044} = 129 \end{aligned}$$

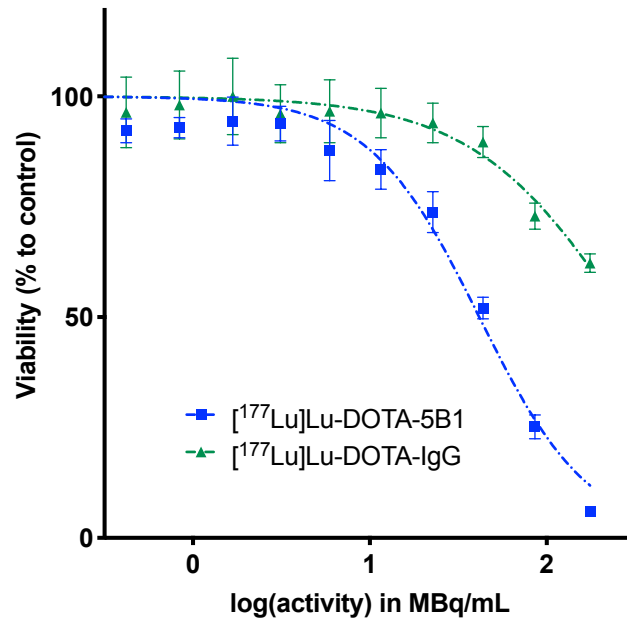


**Figure S1.** *In vitro* cytotoxic potential of  $\beta$ -RIT. Viability of BxPC3 PDAC cells after a 48 hours incubation with various activity concentration of  $[^{177}\text{Lu}]\text{Lu-DOTA-5B1}$  as compared to  $[^{177}\text{Lu}]\text{Lu-DOTA-IgG}$  (n=3 per concentration). Non-specific effect observed here are partly due to cross-fire effect.

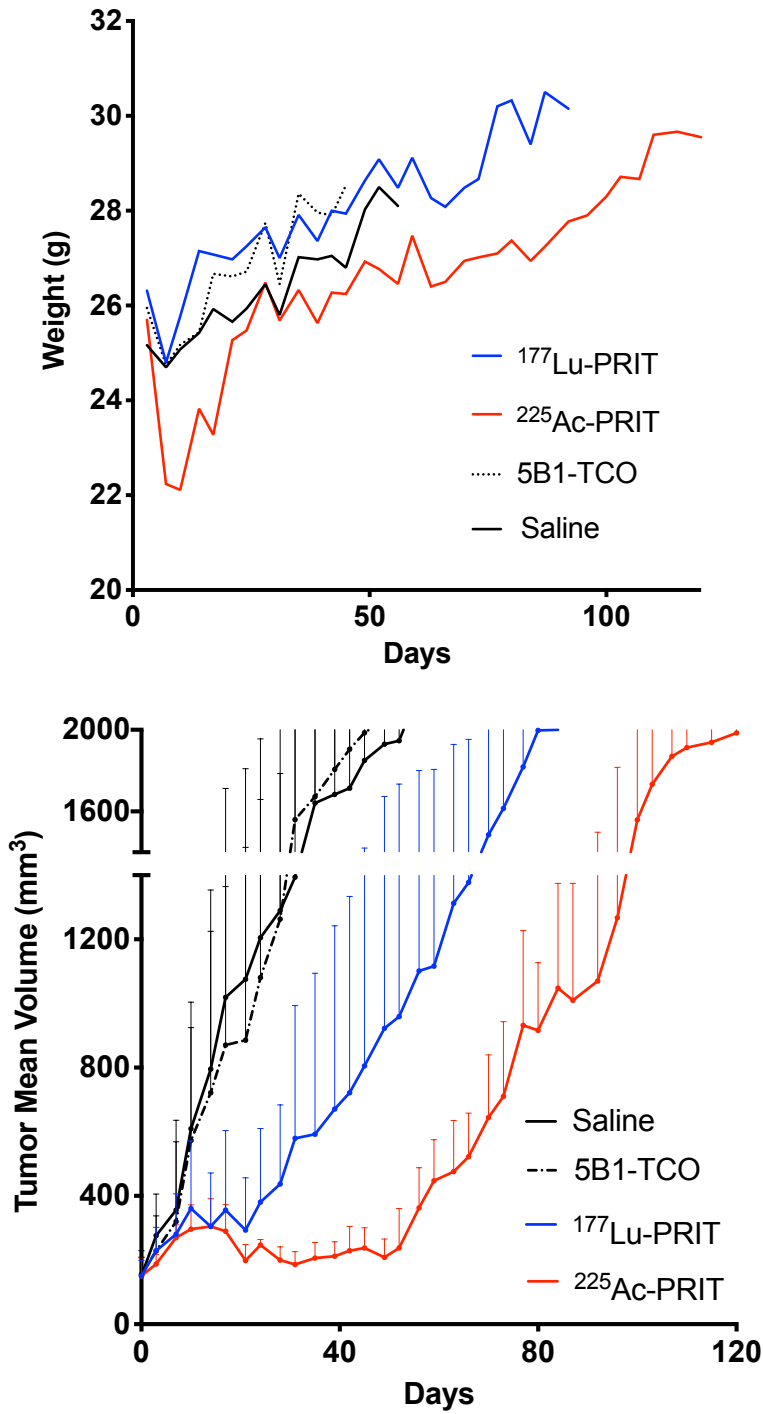


**Figure S2.** Top. Change in body weight during the course of  $\beta$ - and  $\alpha$ -PRIT. Only the mean value at each time point is represented for more clarity. The mean weights values are presented until  $n = 2$  in each cohort. Bottom. Mean tumor volume during the course of  $\beta$ - and  $\alpha$ -PRIT.

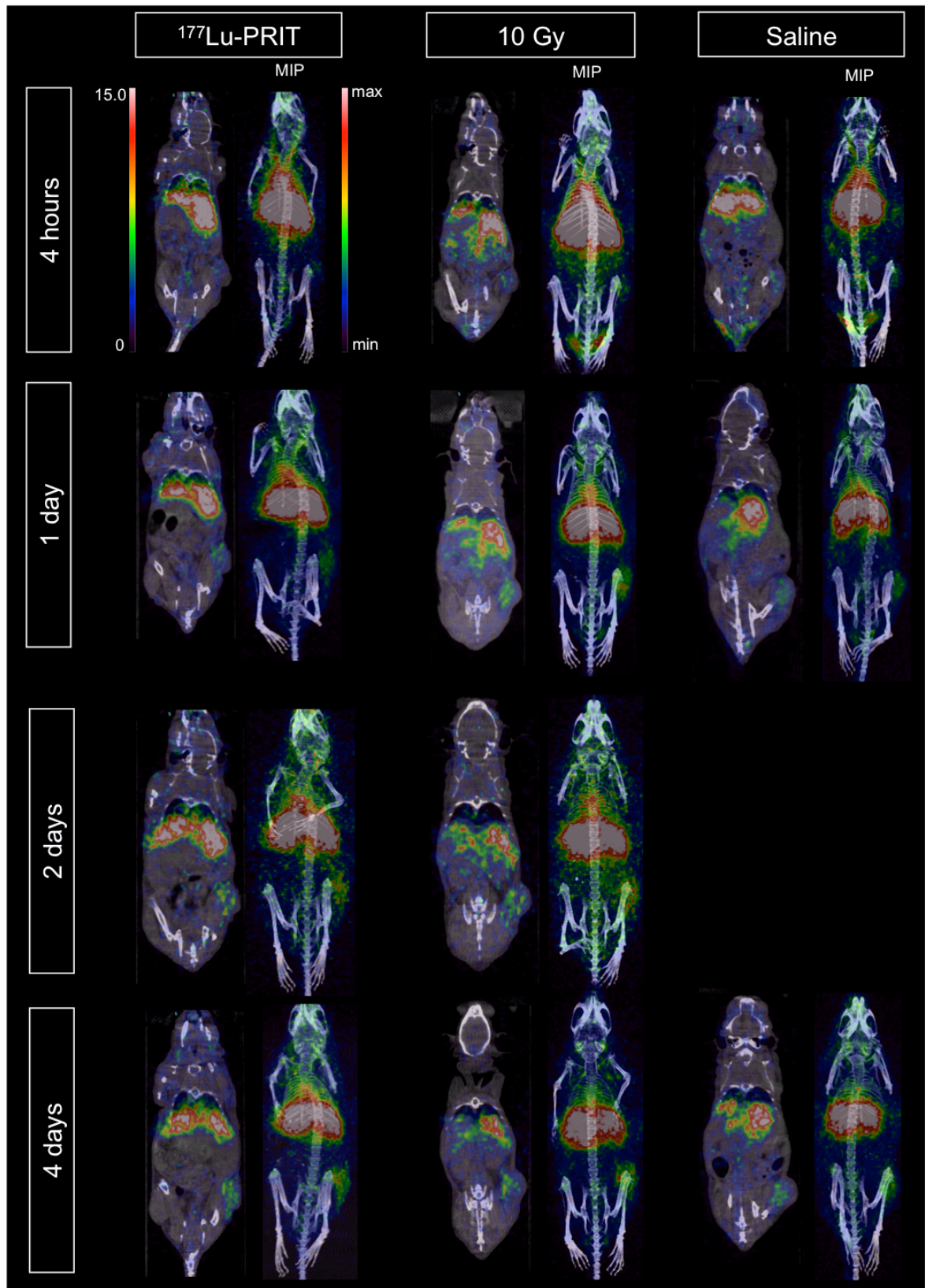


**Figure S3.** PET/CT images showing coronal sections (left) and maximum intensity projections (right) of [ $^{89}\text{Zr}$ ]Zr-DFO-anti- $\gamma\text{H2AX}$ -TAT following  $\beta$ -PRIT in a BxPC3 subcutaneous PDAC xenograft mouse model.

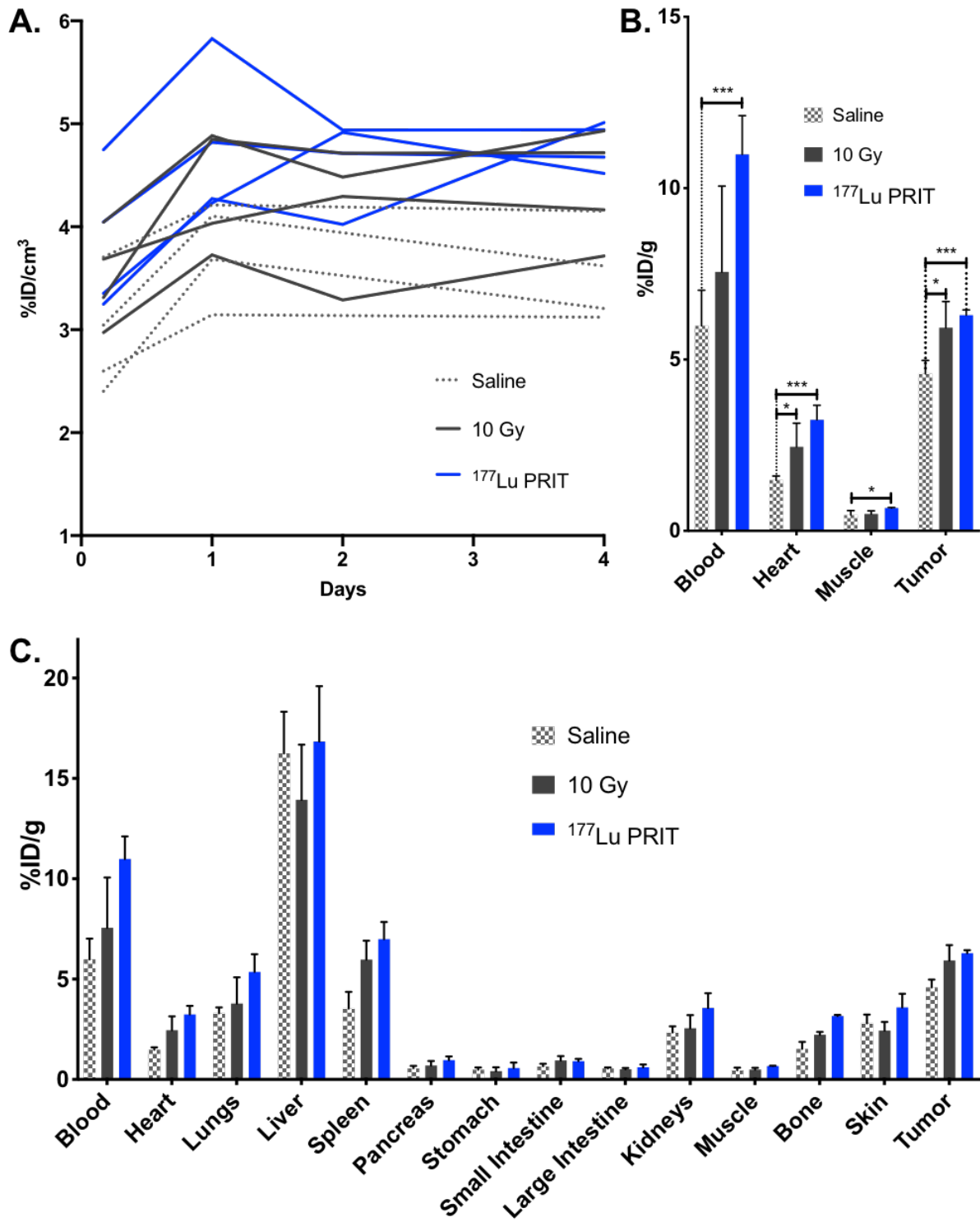


**Figure S4.** In vivo imaging of DNA damage with [<sup>89</sup>Zr]Zr-DFO-anti-γH2AX-TAT following β-PRIT in a BxPC3 subcutaneous PDAC xenograft mouse model. **A.** VOI analysis of tumor [<sup>89</sup>Zr]Zr-DFO-anti-γH2AX-TAT uptake at the different PET/CT imaging time point. **B.** Organ of interest uptake as determined through ex vivo gamma-counting post-animal sacrifice (4 days post-injection of the PET radiotracer). **C.** Full biodistribution profile of [<sup>89</sup>Zr]Zr-DFO-anti-γH2AX-TAT in the different cohorts, 4 days post-injection of the PET radiotracer. Values are represented as means, and error bars represent standard deviations. \*\*\* P ≤ 0.001, \* P ≤ 0.05, n.s. = non significant.

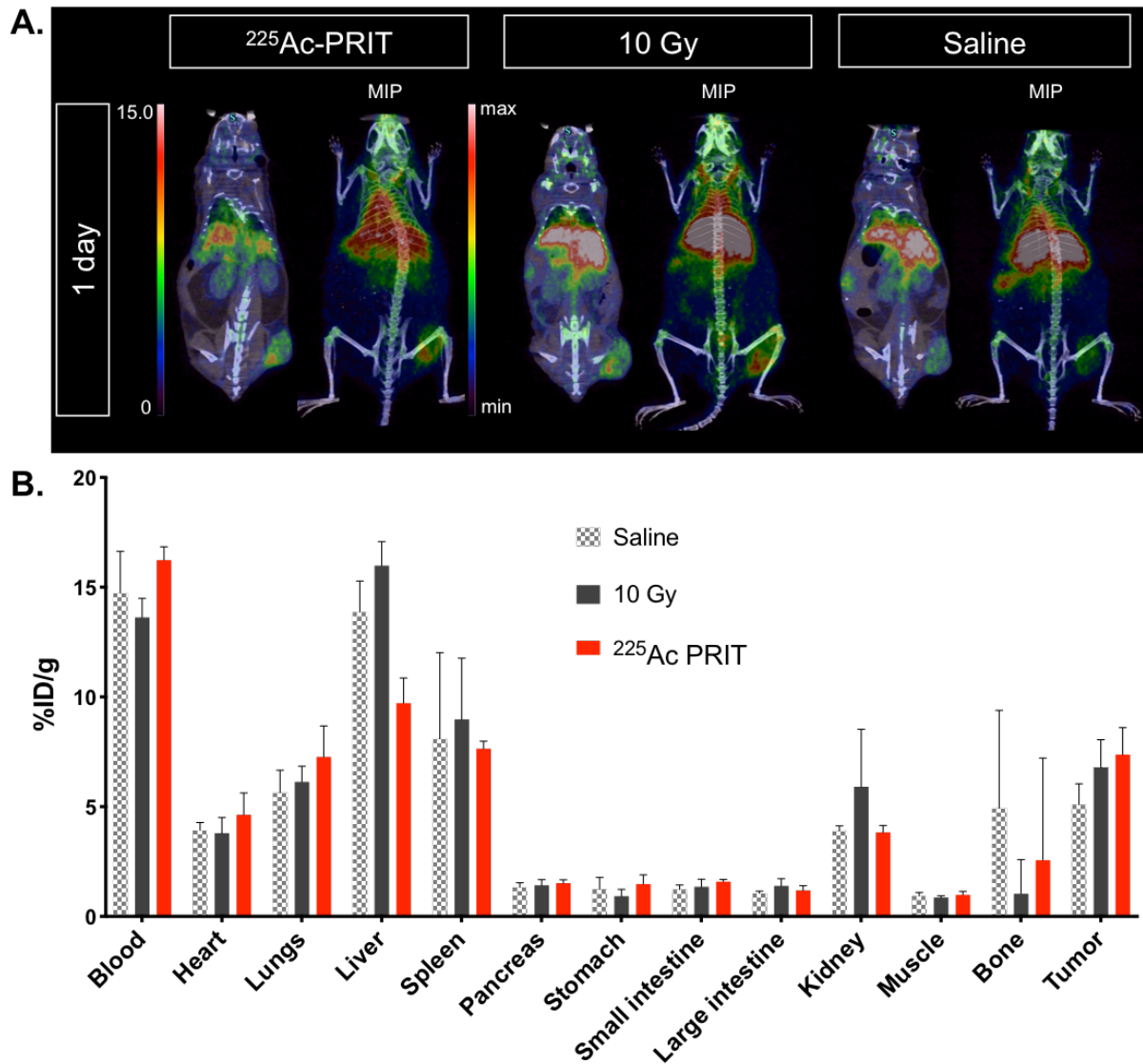


**Figure S5.** In vivo imaging of DNA damage with [<sup>89</sup>Zr]Zr-DFO-anti-γH2AX-TAT following α-PRIT in a BxPC3 subcutaneous PDAC xenograft mouse model. **A.** PET/CT images showing coronal sections (left) and maximum intensity projections (right) of [<sup>89</sup>Zr]Zr-DFO-anti-γH2AX-TAT. **B.** Full biodistribution profile of [<sup>89</sup>Zr]Zr-DFO-anti-γH2AX-TAT in the different cohorts, 24 hours post-injection of the PET radiotracer. Values are represented as means, and error bars represent standard deviations.

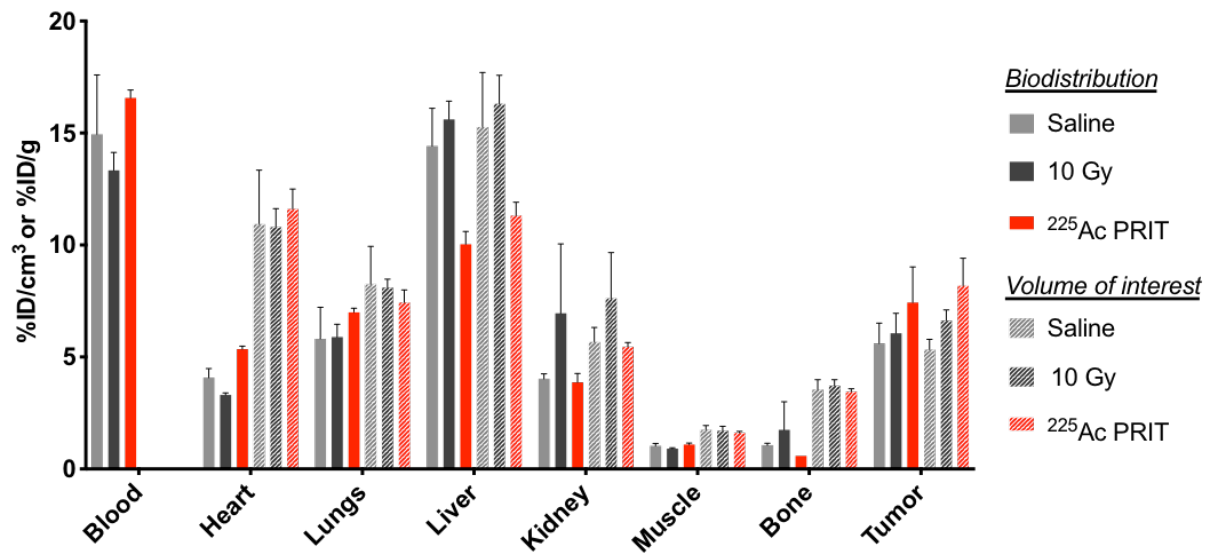


**Figure S6.** Correlation of VOI analysis and organ uptakes as determined through ex vivo gamma-counting post-animal sacrifice with [<sup>89</sup>Zr]Zr-DFO-anti-γH2AX-TAT following α-PRIT in a BxPC3 subcutaneous PDAC xenograft mouse model, 24 hours post-injection of the PET radiotracer.

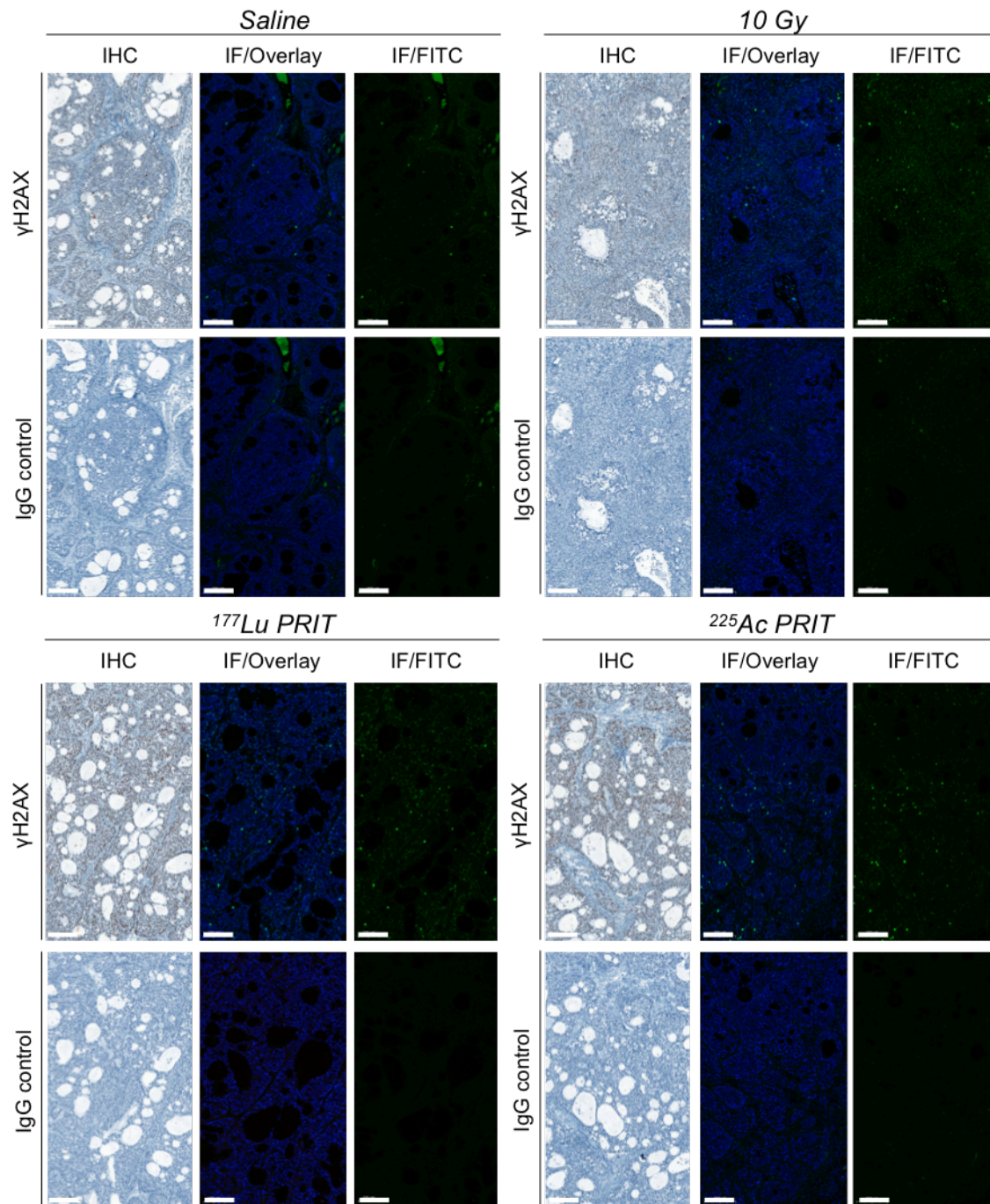


**Figure S7.** γH2AX immunohistochemistry and immunofluorescence staining of BxPC3 mice subcutaneous xenografts treated with saline (negative control), 10Gy EBRT (positive control), β- or α-PRIT. Top images are representative areas of the staining performed with an anti-γH2AX antibody. Bottom images are representative areas of the staining performed with an IgG isotype control. The comparison highlights the specificity of our staining for γH2AX. Scale bar = 200 μm.

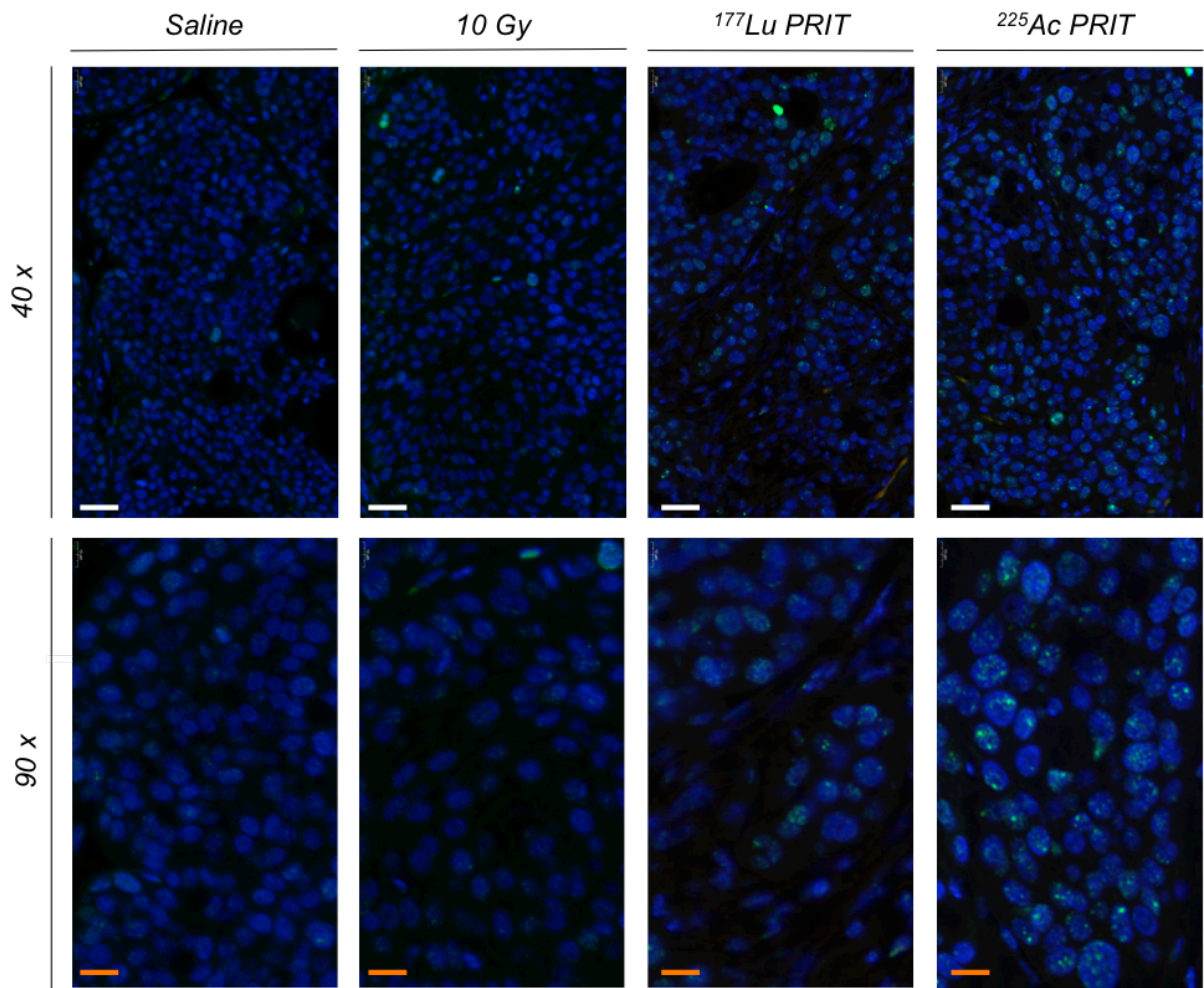


**Figure S8.**  $\gamma$ H2AX immunofluorescence staining of BxPC3 mice subcutaneous xenografts treated with saline (negative control), 10Gy EBRT (positive control),  $\beta$ - or  $\alpha$ -PRIT. White scale bar = 40  $\mu$ m, Orange scale bar = 20  $\mu$ m.